Experimental and simulated control of lift using trailing edge devices

A Cooperman, M Blaylock and C P van Dam

Mechanical and Aerospace Engineering Department, University of California, Davis

E-mail: cpvandam@ucdavis.edu

Abstract. Two active aerodynamic load control (AALC) devices coupled with a control algorithm are shown to decrease the change in lift force experienced by an airfoil during a change in freestream velocity. Microtabs are small (1% chord) surfaces deployed perpendicular to an airfoil, while microjets are pneumatic jets with flow perpendicular to the surface of the airfoil near the trailing edge. Both devices are capable of producing a rapid change in an airfoil's lift coefficient. A control algorithm for microtabs has been tested in a wind tunnel using a modified S819 airfoil, and a microjet control algorithm has been simulated for a NACA 0012 airfoil using OVERFLOW. In both cases, the AALC devices have shown the ability to mitigate the changes in lift during a gust.

1. Introduction

Wind turbine rotor diameters have increased dramatically over the past few decades and their size is expected to continue growing. The continuing growth of these rotors leads to increasing structural and aerodynamic loading on the turbine. Most modern turbines use variable pitch to control loads when they are operating at rated power. The pitch rate for large turbines (5-10 MW) is limited to approximately 6-8°/s. The simplest approach to pitch control is collective pitch, in which all of the blade pitch angles are the same. More advanced controllers include cyclic pitch—in which the blade pitch varies with azimuth angle—and individual pitch control, which allows for non-cyclical variations in pitch angle [1]. Pitch control is limited by the maximum blade pitch rate and by the need to avoid excessive wear on the pitch motors. Active aerodynamic load control can respond quickly to changes in wind speed to reduce the variable loading on the blades and drivetrain [2]. Devices such as trailing edge flaps [3,4], flexible trailing edges [5] and microtabs [6] have been proposed for active load control of wind turbine blades. The two devices chosen for this control system study are microtabs and microjets. Both devices are located near the trailing edge of an airfoil, oriented perpendicularly to the surface. Microtabs are characterized by their height, which is 1-2% of the airfoil chord length. The relevant parameter for microjets is their momentum coefficient, C_μ, which is a function of the jet's width and velocity. Both tabs and jets produce a change in the lift coefficient that shifts the lift curve by a ΔC_L that depends on the device position, size and (for microjets) jet velocity. The response time of both devices is on the order of $t = c/U_\infty$, with 50% of the total ΔC_L occurring in that time period, subject to the device activation speed [7,8]. This provides a potential control system with a fast response to changing conditions.

Although microtabs and microjets are aerodynamically very similar, differences in the actuation of the two devices lead to different choices of control algorithm. The mass flow rate of a jet can be continuously varied to provide a control output that is proportional to the variation in input, which

prompted the selection of proportional-integral-derivative control to test with the microjets. Analogous control of microtabs would require precise monitoring of the tab position and attention to the nonlinearity of ΔC_L with respect to tab height. A simpler feedback control system was chosen for the microtabs in which individual spanwise segments function discretely with each tab either fully deployed or fully retracted.

The application of control systems to microtabs and microjets is part of an ongoing program of research on active aerodynamic load control devices. Both computational and experimental work is being carried out in a complementary fashion. Microjets are being investigated computationally while microtabs are being tested in a wind tunnel. Previous computational work has examined deploying microtabs [7] and ongoing experimental work will provide data on active microjets. All studies are carried out in 2D, which is appropriate to the outboard blade regions where AALC devices are expected to be located. The wind tunnel tests with microtabs are more accurately described as pseudo-2D due to the independent deployment of individual tabs and the presence of gaps between tabs that introduce some three-dimensionality to the model.

2. Methods

2.1. Experimental Setup

The UC Davis Aeronautical Wind Tunnel was used for all tests with active microtabs. The wind tunnel is an open-circuit design driven by a 125 hp AC motor. An electronic speed controller is able to maintain the fan RPM to within ±0.2% of the full scale. The baseline Reynolds number for all tests is 1.0×10^6. A honeycomb and four anti-turbulence screens at the tunnel inlet result in a turbulence intensity of less than 0.1% within 80% of the test section, which measures 0.85 × 1.2 × 3.7 m and incorporates tapered fillets that allow for boundary layer growth and maintain a constant pressure along the test section length. A sealed plenum below the test section houses a six-component pyramidal force balance that is used to measure lift and pitching moment.

The airfoil model used for tests with microtabs is shown in figure 1. It has been designed as a testbed for active load control devices. The S819 airfoil [9] has been modified to double the thickness at 95% chord (c = 0.46 m) to fit a 1% chord height microtab at that location [10]. The model is divided into six spanwise segments that separate to allow access to the hollow interior for installation of sensors and actuators. The aft 47% of each section can be removed and different trailing edge devices can be installed. For these tests, microtabs were installed at 90% chord on the upper surface (suction side) and 95% chord on the lower surface (pressure side). The tabs retract fully into the airfoil; when deployed the upper surface tab height is 0.9% c (3.9 mm) and the lower surface tab height is 1.0% c

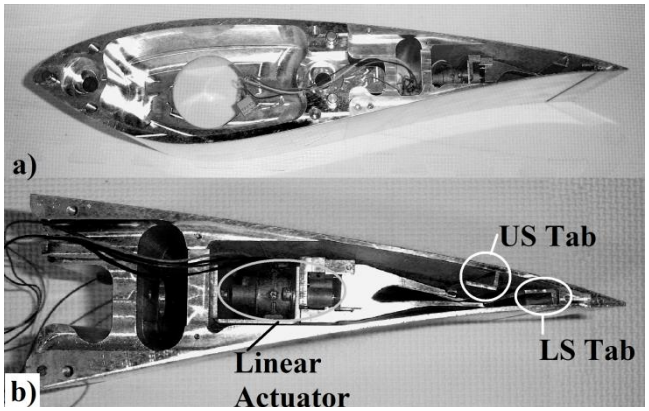

Figure 1. **(a)** Cross-section of modified S819 profile (S819m) used for microtab testing **(b)** aft section of model with tabs.

(4.5 mm). Each of the six tabs on either surface is 127 mm in the spanwise direction and is separated from adjacent tabs by a 9 mm gap. The total span of the model is 0.84 m, with 3 mm clearance between the model and the floor of the wind tunnel and 7 mm clearance at the top of the model.

Each of the twelve tabs is driven by a 1.2 watt linear actuator. The tabs are operated in a binary fashion in which each tab is either fully deployed or fully retracted. The time required for a single tab to be deployed is 0.2 s. During a simulated gust, tabs operate on only one surface, upper or lower, while tabs on the other surface are retracted with the surface slots covered to prevent cross-flow.

Surface pressure is measured at two locations using Endevco 8507C-1 pressure transducers, which are mounted directly below the model surface at 15% chord on the upper and lower surfaces. The transducer location was chosen based on two criteria: sensitivity to changes in lift and space for installation. The transducers' range is ±1.0 psi and they are accurate to within 1% of the full scale, with a flat frequency response up to 11 kHz. The transducers provide a highly accurate sensor for the control system due to their fast response time and proximity to the airfoil surface.

2.2. Computational Methods

The unsteady RANS flow solver OVERFLOW [11-14] was used to conduct the 2D computational investigation of microjets as AALC devices. The case was run run fully turbulent using the Menter's SST *k-ω* turbulence model and was performed with second order time accuracy and dual time stepping. The force and moment coefficients were calculated using the FOMOCO utilities [15]. The effect of the jet on these calculations is described in detail in [16]. Using Chimera Grid Tools [17-19], the jets are placed near the trailing edge (x/c = 0.95) on both the suction (upper) surface and pressure (lower) surface of a NACA 0012 airfoil. Figure shows activation of the pressure surface jet. The simulations were run at a Reynolds number of $Re = 1.0 \times 10^6$ and a Mach number of Ma = 0.15.

The microjets are characterized by the non-dimensional momentum coefficient, C_μ. This term relates the jet momentum to the free stream momentum and is defined as [20]:

$$C_\mu = \frac{\dot{m}_{jet}\, U_{jet}}{\frac{1}{2}\rho_\infty U_\infty^2 S} \tag{1}$$

where $\dot{m}_{jet} = \rho_{jet} U_{jet} A_{jet}$ is the mass flow rate of the jet**,** U_{jet} is the average velocity of the jet measured at the exit**,** ρ_∞ and U_∞ are the freestream air density and velocity, and S is the planform area of the blade section. The jet exits normal to the wall of the airfoil as an inflow velocity boundary condition with the magnitude determined by a PI controller describe in section 4.2.

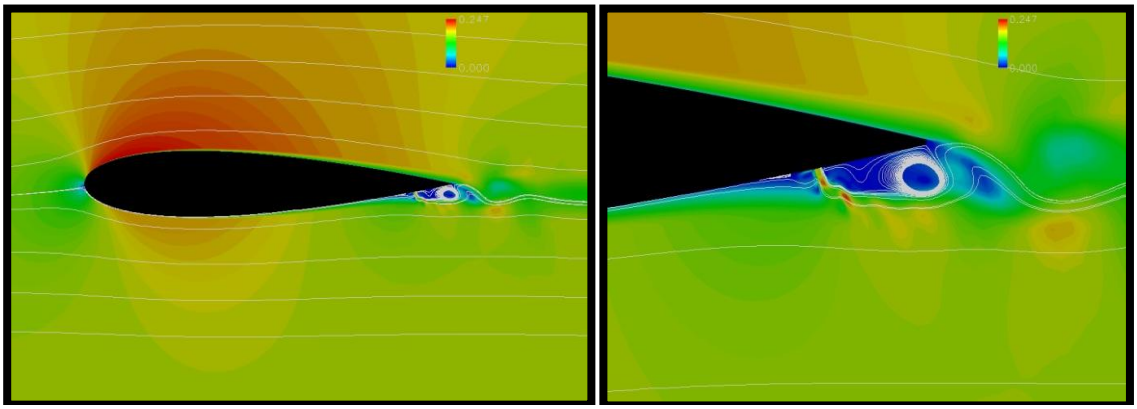

Figure 2. OVERFLOW simulation showing the flow velocity and instantaneous streak lines around an airfoil with an activated pressure side jet, $\alpha = 0°$, $Re = 1.0 \times 10^6$.

The non-dimensional characteristic time unit, T, is defined as $T = U_\infty t/c$, which takes a value of unity for t = 0.02 s, U_∞ = 50 m/s, and chord c = 1 m. A gust which lasted 10T (over 10,000 time steps) was created by increasing the incoming free stream velocity by 13% from the baseline air speed in five characteristic time units and then back to the baseline in another five time units. This rather short gust

was selected to allow for more simulations. Longer gusts, on the order of 10 s, require very long simulation times, making it difficult to evaluate and optimize control algorithms.

The grid has two components: a body grid and a far field grid. The body grid is a 749 × 378 node C-grid that has 570 nodes around a NACA 0012 airfoil and 90 nodes in the wake. There are 53 nodes across each of the jet locations, which are placed at x/c = 0.95. The jet widths are h_{jet} = 0.005c. The entire body grid is tilted to have an angle of attack of 4˚, which causes the incoming gust to hit the airfoil at α = 4˚. The far field grid is a rectangle that has 252 × 159 nodes. It extends in front, above and below the airfoil for 50c and behind the airfoil 225c. The first four grid spacings nearest the wall around the airfoil are calculated to be smaller than y^+ = 1 at the specified chord Reynolds number. The boundary condition for the gust was created by setting a time varying inflow condition on the left hand side of the rectangle. The top, bottom and right hand side of the rectangle had outflow boundary conditions.

3. Control systems

Control systems were developed for the microjet and microtab airfoils. Although the actuation systems are different, the same two inputs were used for both systems: a direct measurement of lift force and a derived lift force based on the pressure difference between the upper and lower surface at a single chordwise location. The objective of both control systems is to minimize the change in lift force during changes in atmospheric conditions.

3.1. Surface pressure based lift sensor

Both microtabs and microjets operate by altering the lift curve of an airfoil; however, the sectional lift coefficient is not a quantity that is easily measured on an operating wind turbine. The lift coefficient can be approximated using the difference in pressure between the upper and lower surfaces of an airfoil at a single chordwise location [21,22]. For an airfoil without AALC devices operating in the linear lift regime, a linear relationship can be found between the lift coefficient and the pressure difference coefficient, ΔC_P. For finite thickness airfoils this provides a reasonable approximation for locations where the slope of the camberline is small ($\ll$1). Pressure measurements are taken at 15% chord on the S819m airfoil and 25% chord on the NACA 0012 airfoil. The relationship between lift force and surface pressure difference at either location is expected to be linear, although the slope varies with chordwise location and airfoil camber. The relationship between C_L and ΔC_P at 25% chord ($\Delta C_{P,25}$) is shown in figure 3 for the NACA 0012 airfoil. A linear fit to the data in figure 3 yields the trend line:

$$C_L = 1.5462 * \Delta C_{P,25} - 0.0192 \quad (2)$$

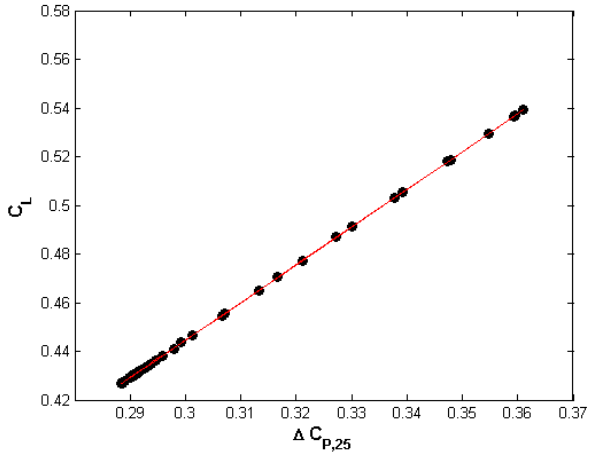

Figure 3. Coefficients of lift and pressure difference at x/c = 0.25 for the NACA 0012 airfoil.

3.1.1 Microtab lift sensor. Figure 4 shows C_L and $\Delta C_{P,15}$ for the S819m airfoil without tabs as well as the airfoil with a 1.1% chord height gapless tab on either surface, measured while varying the angle of attack between 0° and 10°. No roughness elements were used to change the boundary layer transition location. The deployment of tabs does not change the slope of the relationship between C_L and $\Delta C_{P,15}$ significantly, but it shifts the intercept upwards for lower surface tabs and downwards for upper surface tabs. Deployments of individual tabs confirm that the offset is proportional to the number of tabs deployed. Taking the average slope and dividing the difference in intercepts equally between the tabs on each surface results in the following equation for the lift coefficient derived from $\Delta C_{P,15}$:

$$C_{L\Delta P} = 0.45\,\Delta C_{P,15} + 0.11 + 0.015\,n_{tabs} \quad (3)$$

where n_{tabs} is the number of tabs deployed and runs from -6 to 6, with negative values denoting upper surface tabs. Multiplying equation (3) by the dynamic head, q_∞ (in Pa), and the model planform area returns an equation for the physically measured quantities of lift (in N) and ΔP_{15} (in Pa):

$$L_{\Delta P} = 0.17\,\Delta P_{15} + 0.043\,q_\infty + 0.0035\,q_\infty n_{tabs} \quad (4)$$

3.1.2 Microjet lift sensor. To determine how microjet activation changes the relationship between C_L and $\Delta C_{P,25}$, a test was conducted where the upper surface jet velocity was ramped from zero to U_∞. The test was run at $Re = 1.0 \times 10^6$ and $Ma = 0.15$ on the NACA 0012 airfoil at $\alpha = 4^\circ$. Figure 5 shows the lift (thick line) and the pressure (dashed line) during this test, as well as the lift derived from equation (2) (thin line). By using the difference between the derived lift and the actual lift, offsets for two different jet velocity regimes were determined. The second regime, $U_{jet}/U_\infty > 0.6$, coincides with the velocities at which vortex shedding produces oscillations in the lift [1616]. These offsets are then added to equation (2) to get the final derived lift value. The trend line for offset1 (thin dashed line in figure 5), which is used when $0.1 < U_{jet}/U_\infty < 0.6$, is:

$$\text{offset1} = -0.0966 * U_{jet}/U_\infty - 0.0054 \quad (5)$$

The trend line for offset2 (dot dashed line), which is implemented when $U_{jet}/U_\infty > 0.6$, is:

$$\text{offset2} = -0.0157 * U_{jet}/U_\infty - 0.0525 \quad (6)$$

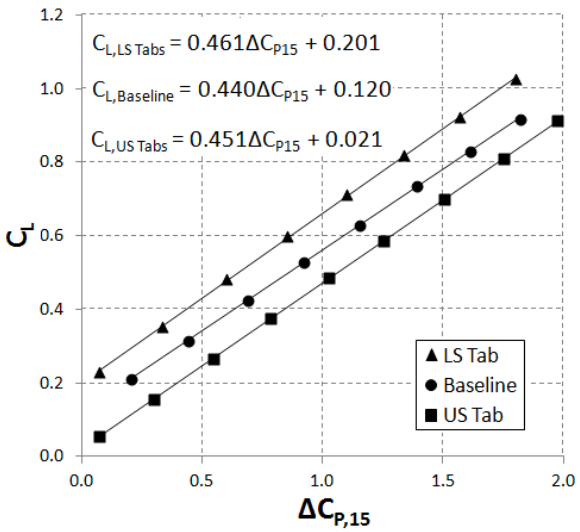

Figure 4. Lift coefficient and pressure difference coefficient for the S819m airfoil with no tabs (baseline), upper surface tab and lower surface tab. Linear fits are shown for each data set.

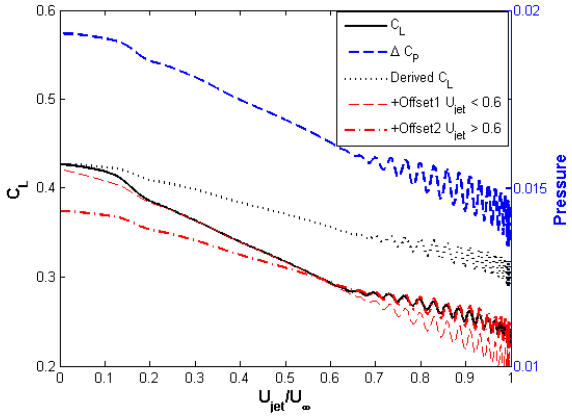

Figure 5. Lift, pressure difference and derived lift coefficients for the NACA 0012 airfoil with upper surface jet.

3.2. Microtab control system

The control system for the tabs is a simple feedback controller with a deadband. Before beginning a control run, the setpoint, L_o, is determined based on an average value of the lift force over a period of 2.5 s. The controller evaluates the error, $e(t) = L_o - L(t)$, between the setpoint and the input lift force, updating at a frequency of 20 Hz. If the error is larger than a given margin, Δ_L, the control system deploys or retracts the next tab in sequence, choosing the activation direction that will reduce the error. If all tabs on a surface are already deployed, no action is taken. Only one tab can be activated during an iteration of the control loop. With the controller operating at a frequency of 20 Hz and a tab activation time of 0.2 s, the minimum time between tab deployments is 0.25 s. A flowchart illustrating the control system for tabs on the lower surface is shown in figure 6.

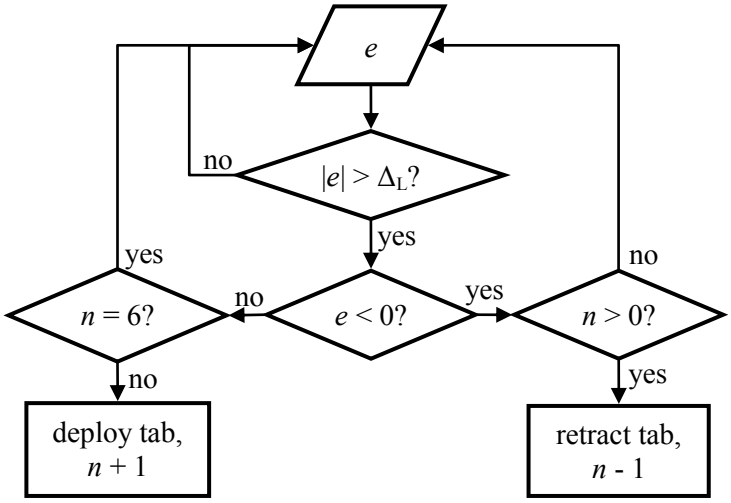

Figure 6. Control system flowchart for tabs on lower surface ($n \geq 0$).

3.3. Microjet control system

A Proportional-Integral-Derivative (PID) controller was chosen for the initial design of the microjet control system due to its widespread use throughout industry today [23]. It was found that a PI controller works well for this application.

As the name suggests, Proportional-Integral-Derivative controllers have three parts to the value of the output signal: one that is proportional to the error, one that is based on the integral of the error over time, and one that is based on the derivative of the error:

$$U_{jet}(t) = K_P e(t) + K_I \int e(t)dt + K_D \frac{de(t)}{dt} \quad (7)$$

For the control of a microjet, the output, $U_{jet}(t)$, determines the velocity of the jet. If $U_{jet}(t)$ is negative, then the jet velocity is set to zero, otherwise the jet velocity is set to equal $U_{jet}(t)$. Hand tuning of the three gains was completed, and the following values were obtained: $K_P = 1.5$, $K_I = 2.0$, and $K_D = 0.0$. The same values for the gains were used on both the upper and lower surface jets, as well as for both control system inputs, lift and lift derived from the pressure difference.

4. Results

4.1. Microtabs

The tab control system was tested by introducing air speed changes in the wind tunnel. Each simulated gust begins at a Reynolds number of 1.0×10^6, which corresponds to a test section air speed of approximately 34 m/s for this model in typical atmospheric conditions. The size of the gusts ranged from 2 to 9 m/s, both increasing and decreasing the air speed. Gusts were repeated without control for comparison with the controlled performance. During each gust, the air accelerated smoothly from the

baseline speed at a rate of 2 m/s^2. In the time series shown in figures 7 and 8 below, each gust begins at t = 2.9 s.

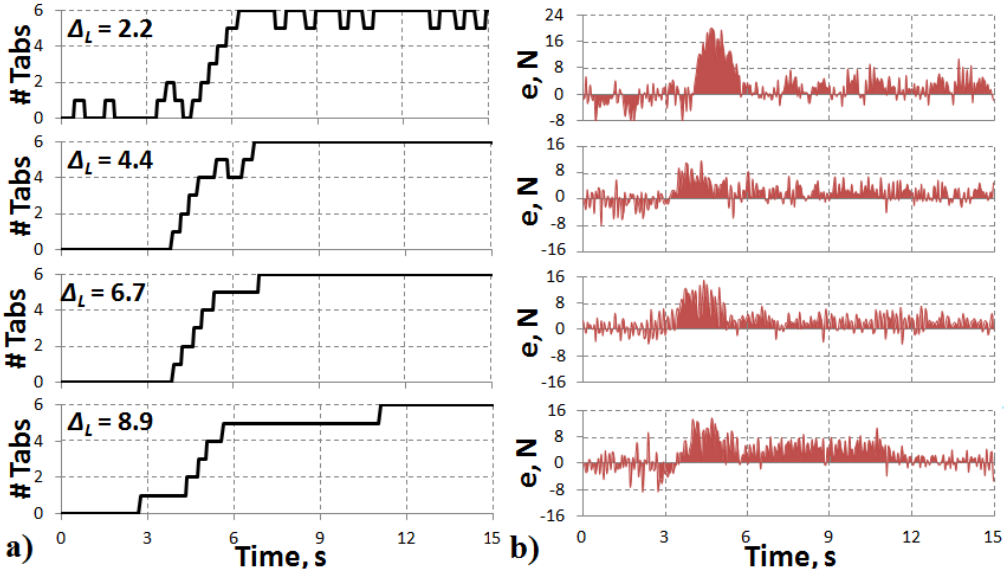

Figure 7. Sample time series of (a) tab activity and (b) lift error for varying control margin, Δ_L, in N. Tabs on lower surface, α = 3°, air speed change ΔU_∞ = -4.5 m/s at t = 2.9 s.

Initially, lift measured by the force balance ($L_{balance}$) was used as the input to the control system. A range of control margin sizes were tested to determine the optimal margin for this system, with four sample time series given in figure 7. A small margin provides a more rapid response to changing airspeed, but also results in tab activations in response to random noise in the lift signal as seen for Δ_L = 2.2 N in figure 7. Conversely, a large margin avoids unnecessary tab activations, but does not respond as quickly to a change in air speed. The best control was obtained for a margin of 4.4 N. This value is close to the average lift change of 5.3 N produced by a single tab at the baseline Reynolds number.

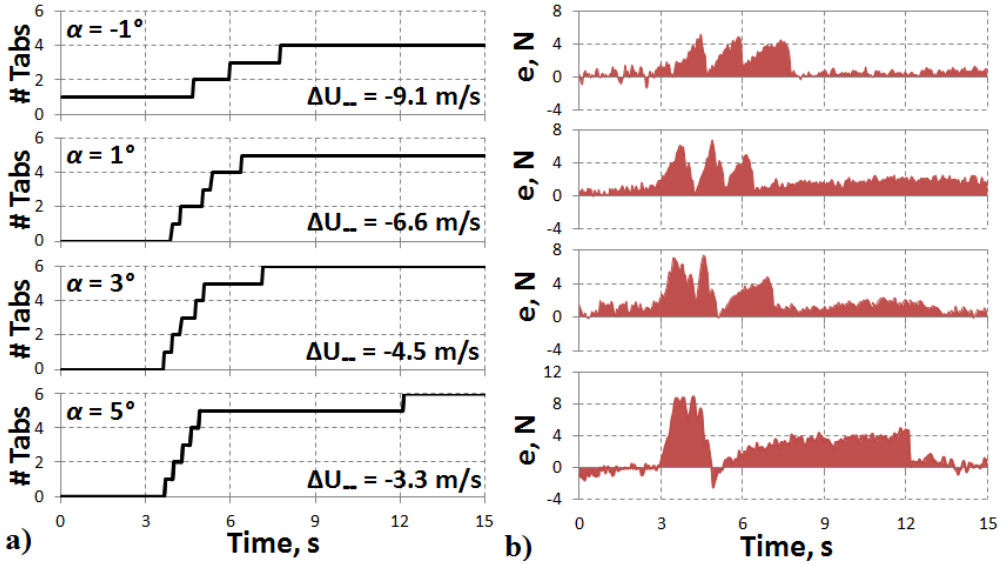

Figure 8. Sample time series of (a) tab activity and (b) lift error for varying angles of attack. Tabs on lower surface, control margin Δ_L = 3.3 N, ΔU_∞ at t = 2.9 s.

The control input was changed from lift force measured by the balance to lift force derived from the pressure difference at 15% chord, $L_{\Delta P}$. Figure 8 shows tab activity and error, e, based on derived lift values for four different angles of attack. The control system based on $L_{\Delta P}$ does not exhibit excessive tab activation like that seen for small control margins with the $L_{balance}$-based control; the number of tabs increases monotonically in each case. Fewer tabs activate at lower angles of attack because the total change in lift force is smaller: -12 N at α = -1° compared with -29 N at α = 7° for the respective uncontrolled cases. The error based on $L_{\Delta P}$ is smaller than the error based on $L_{balance}$ (note difference in scale between figure 7b and figure 8b) due to the lower level of noise in the surface pressure signal.

In figure 9, control based on $L_{balance}$ is compared with control based on $L_{\Delta P}$ for a range of angles of attack and control margins. The quantity used to compare the two systems is the total error

$$E = \int \left| L_{balance}(t) - L_o \right| dt \tag{8}$$

which is normalized by the total error for the corresponding uncontrolled case at each angle of attack. Note that lift from the force balance is used to evaluate both control systems in order to eliminate differences due to the signal quality or errors in the derived lift force. Overall, the two control systems perform similarly, reducing the total error by 70-80% in most cases compared with the uncontrolled airfoil. Less reduction is seen at α = -1° because the total error in the uncontrolled case is smaller than for the other angles of attack. The largest reduction in total error is seen for $\Delta_{L,\Delta P}$ = 3.3 N at α = 1°, in which E with control is 81.9% less than E for the uncontrolled case.

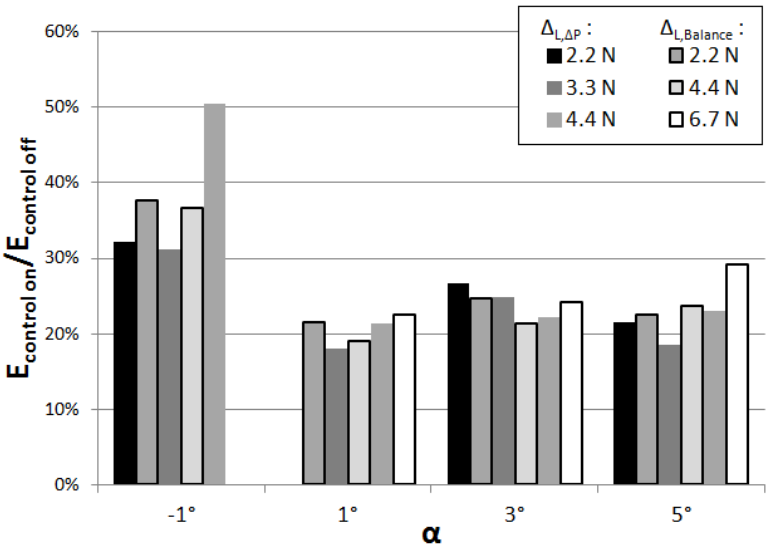

Figure 9. Total error for tab-controlled cases as a percentage of total error in uncontrolled cases. Several control margins, Δ_L, are compared at each angle of attack. Input to tab control system is lift force measured by force balance (dark outline) or derived from the surface pressure difference at x/c = 0.15 (no outline).

4.2. Microjets

CFD simulations of a gust with duration 10T and a 13% increase in U_∞ were conducted both with and without the PI-controlled microjets. In figure 10, the solid black line shows the change in lift force per unit span (normalized using the undisturbed far-field dynamic head and airfoil chord, $\frac{1}{2}\rho U_\infty^2 c$) due to the 10$T$ gust without microjets, and the dotted line shows the lift during the same gust when the microjets are used. Using the same metric to quantify the reduction in the change in lift as is described for the microtabs, the total error with the microjets is 34.4% of the total error without the microjets.

Figure 11 shows the microjet momentum coefficients to achieve this result. The solid line indicates the activation of the suction side jet, and the dotted line shows the pressure side jet. Since the gust increases the lift force, the suction side jet is activated more than the pressure side jet, for which the momentum coefficient remains comparatively very low.

The test was then repeated using the lift derived from the pressure difference at 25% chord to control the jet velocities. As can be seen from figure 12, applying the correction based on the jet velocity improves the control system performance. Without the corrections (thin line in figure 12), the total error is 64.2% of the total error without the microjets. When the corrections are made, the normalized total error is reduced to 42.9%.

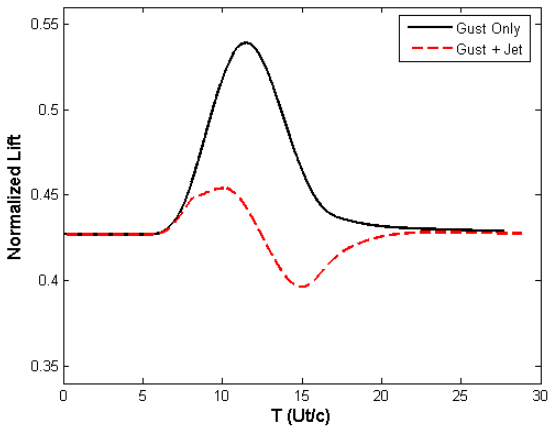

Figure 10. The change in lift with the microjets (dashed line) is less than the change in lift from the gust without microjets (solid line).

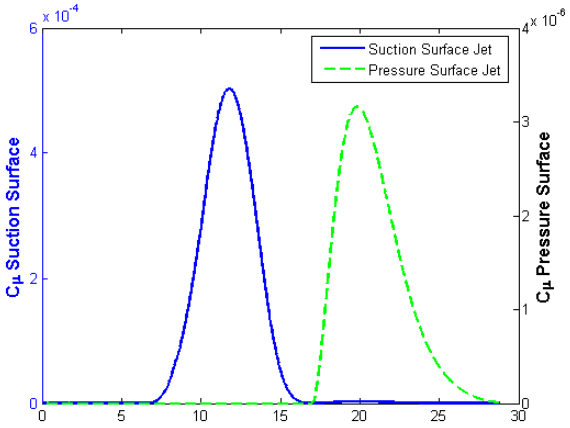

Figure 11. Momentum coefficient for the 10*T* gust for both the suction and pressure surface jets. Note that the momentum of the suction surface jet is over two orders of magnitude larger than that of the pressure surface jet.

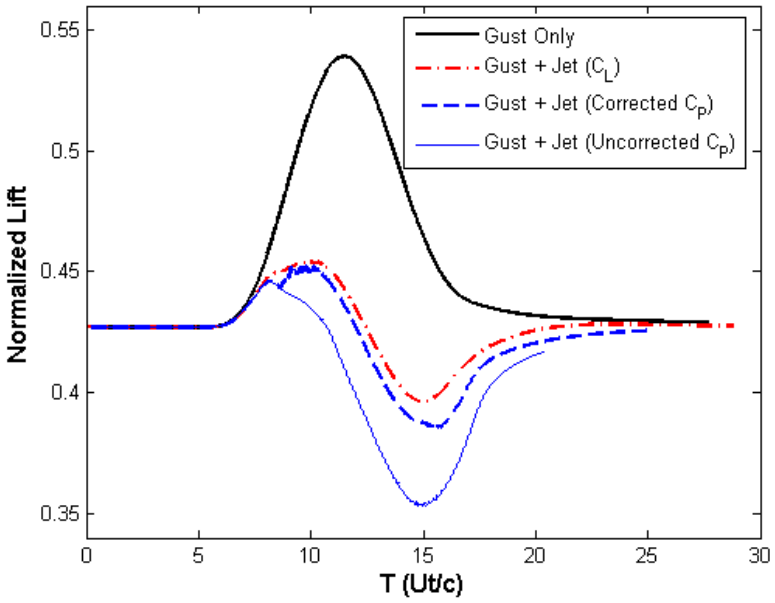

Figure 12. The reaction of the lift to a 10*T* gust without microjets (thick black line), with microjets that have a PI controller based on lift (dot dashed line), with microjets that have a PI controller based on lift derived from the pressure (thin line), and with microjets that have a PI controller based on the lift derived from the pressure with the offsets described in the text (thick dashed line). Adding the correction based on the jet velocity improved the performance of the control algorithm.

5. Conclusions

Control systems have been developed using microtabs and microjets that reduce the variation in lift force of an airfoil subjected to changes in air speed. Two different inputs were tested for these control systems: direct lift measurements and lift force derived from the difference in surface pressure at a single chordwise location. Wind tunnel tests at constant angles of attack between -1–5˚ found that a feedback controller using microtabs can reduce the deviation from the desired value of lift by 70%–

80% compared to the uncontrolled airfoil during a change in the test section air speed. The CFD results for the microjet indicate that this device can also reduce the lift error by around 65% for $\alpha = 4^{\circ}$ when direct lift measurement is used as input to a PI controller. A slightly smaller reduction of 57% is achieved when the lift is derived from pressure measurements on the airfoil.

Acknowledgements
The authors would like to thank the Wind Energy Technologies Program of Sandia National Laboratories, the NSF GK-12 Program, and the Warren and Leta Giedt Endowment for their support.

References

[1] Bossanyi, E A 2003 Wind turbine control for load reduction *Wind Energy* **6** 229–244
[2] Johnson S J, Baker J P, van Dam C P and Berg D 2010 An overview of active load control techniques for wind turbines with an emphasis on microtabs *Wind Energy* **13** 239–53
[3] Basualdo, S 2005 Load alleviation on wind turbine blades using variable airfoil geometry *Wind Engineering* **29** 169–182
[4] Van Wingerden J W, Hulskamp A W, Barlas T, Marrant B, van Kuik G A M, Molenaar D-P, and Verhaegen M 2008 On the proof of concept of a "smart" wind turbine rotor blade for load alleviation *Wind Energy* **11** 265–280
[5] Bak C, Gaunaa M, Andersen P, Buhl T, Hansen P, Clemmensen K, and Moeller R 2007 Wind tunnel test on wind turbine airfoil with adaptive trailing edge geometry *45th AIAA Aerospace Sciences Meeting (Reno, NV, 8-11 January 2007)* AIAA 2007-1016
[6] Yen Nakafuji D T, van Dam C P, Smith R L, and Collins S D 2001 Active load control for airfoils using microtabs *Journal of Solar Energy Engineering* **123** 282–298
[7] Chow R and van Dam C P 2006 Unsteady computational investigations of deploying load control microtabs *J. Aircraft* **43** 1458–69
[8] Boeije C S, de Vries H, Cleine I, van Emden E, Zwart G G M, Stobbe H, Hirschberg A and Hoeijmakers H W M 2009 Fluidic load control for wind turbine blades *47th AIAA Aerospace Sciences Meeting (Orlando, FL, 5-8 January 2009)* AIAA 2009-684
[9] Somers D M 2005 The S819, S820, and S821 airfoils *National Renewable Energy Laboratory Subcontractor Report* 500-36334
[10] Cooperman A M, Chow R, and van Dam C P 2013 Active load control of a wind turbine airfoil using microtabs *Journal of Aircraft* **50** 1150–58
[11] Buning P G, Jesperson D C, Pulliam T H, Chan W M, Soltnick J P, Krist S E and Renze K J 2003 OVERFLOW User's Manual, Version 1.8ab NASA Langley Research Center
[12] Jespersen D, Pulliam T and Buning P 1997 Recent enhancements to OVERFLOW *35th Aerospace Sciences Meeting (Reno, NV, 6-9 January 1997)* AIAA 1997-0644
[13] Nichols R H and Buning P G 2008 User's manual for OVERFLOW 2.1 NASA Langley Research Center, Hampton, VA
[14] Meakin R L 2001 Object x-rays for cutting holes in composite overset structured grids *15th AIAA Computational Fluid Dynamics Conference* (*Anaheim, CA, 11-14 June 2001*) AIAA-2001-2537
[15] Chan W M and Buning P G 1996 *User's Manual for FOMOCO Utilities - Force and Moment Computation Tools for Overset Grids* NASA Ames Research Center
[16] Blaylock M, Chow R, Cooperman A, and van Dam C P 2013 Comparison of pneumatic jets and tabs for active aerodynamic load control *Wind Energy* doi:10.1002/we.163
[17] Chan W M 2002 Overgrid interface for computational simulations on overset grids *40th AIAA Aerospace Sciences Meeting and Exhibit (Reno, NV*) AIAA-2002-3188
[18] Chan W M, Gomez R J, Rogers S E and Buning P G 2002 Best practices in overset grid generation *32nd AIAA Fluid Dynamics Conference and Exhibit (St. Louis, MO, 24-26 June 2002)* AIAA-2002-3191

[19] Chan W M, Rogers S E, Nash S M, Buning P G and Meakin R L 2003 User's manual for chimera grid tools, Version 1.8 NASA Ames Research Center, Moffet Field, CA
[20] Lachmann G V 1961 *Boundary Layer and Flow Control: Its Principles and Application* vol 1 (Oxford: Pergamon)
[21] Gaunaa M and Andersen P B 2009 Load reduction using pressure difference on airfoil for control of trailing-edge flaps *Proc. European Wind Energy Conference (Marseille, 16-19 March 2009)*
[22] Gaunaa M 2010 Unsteady two-dimensional potential-flow model for thin variable geometry airfoils *Wind Energy* **13** 167–92
[23] Visiloi, A 2006 *Practical PID Control* (London: Springer-Verlag)